Magn Reson Med Sci 2021; 20; 60–68
doi:10.2463/mrms.mp.2019-0195
Published Online: March 6, 2020

MAJOR PAPER

Turbo Spin-echo Diffusion-weighted Imaging Compared with Single-shot Echo-planar Diffusion-weighted Imaging: Image Quality and Diagnostic Performance When Differentiating between Ductal Carcinoma *in situ* and Invasive Ductal Carcinoma

Naoko Mori[1*], Shunji Mugikura[1], Minoru Miyashita[2], Yu Mori[3], Yui Maekawa[1], Tatsuo Nagasaka[4], and Kei Takase[1]

Purpose: To compare the image quality between turbo spin-echo (TSE)-diffusion weighted imaging (DWI) and single-shot echo-planar imaging (EPI)-DWI, and to verify the diagnostic performance of the apparent diffusion coefficient (ADC) parameters of the two techniques by using histogram analysis in terms of differentiation between ductal carcinoma *in situ* (DCIS) and invasive ductal carcinoma (IDC) lesions.

Methods: Ninety-four women with 94 lesions diagnosed as breast cancer by surgery underwent IRB-approved preoperative magnetic resonance imaging, including TSE and EPI-DWI with *b*-values of 50 and 850 s/mm^2. Twenty lesions were identified as DCIS and 74 as IDC. Image quality [signal-to-noise ratio (SNR), contrast-to-noise ratio (CNR), and geometric distortion] was evaluated quantitatively and compared between the TSE and EPI-DWI. A histogram analysis of the entire tumor voxel-based ADC data was performed, and the 10th, 25th, 50th, 75th, and 90th percentile values of each technique were compared between DCIS and IDC lesions.

Results: The SNR and CNR of TSE-DWI were significantly higher than those of EPI-DWI ($P < 0.0001$ and < 0.0001). The geometric distortion of TSE-DWI was significantly lower than that of EPI-DWI ($P < 0.0001$). In TSE-DWI, the 10th, 25th, 50th, and 75th percentile values were significantly different between the DCIS and IDC lesions ($P = 0.0010$, 0.0004, 0.0008, and 0.0044, respectively). In EPI-DWI, the 50th and 75th percentile values were significantly different between the two groups ($P = 0.0009$ and 0.0093). There was no significant difference in the area under the curve of the receiver operating characteristic analysis of the 10th, 25th, 50th, and 75th percentile values of TSE-DWI, and the 50th and 75th percentile values of EPI-DWI ($P = 0.29$).

Conclusion: The image quality of TSE-DWI was better than that of EPI-DWI. DCIS lesions were distinguished from IDC lesions with a wider range of percentile values in TSE-DWI than in EPI-DWI, although diagnostic performance was not significantly different between the techniques.

Keywords: *breast cancer, diffusion weighted imaging, Turbo spin-echo, ductal carcinoma* in situ*, invasive ductal carcinoma*

Introduction

Apparent diffusion coefficient (ADC) values calculated from the signal intensity of diffusion-weighted imaging (DWI) are considered to reflect the degree of diffusion of water molecules.[1,2] Previous studies have reported the utility of ADC values for differentiating benign from malignant breast lesions,[3–5] grading breast cancer,[1,6–8] and evaluating responses to neoadjuvant chemotherapy.[9–11] For grading breast cancer, the differentiation between ductal carcinoma *in situ* (DCIS) and invasive ductal carcinoma (IDC) is important because management and prognosis are different between the two groups.[12–14] Several studies have reported that the ADC values of IDC lesions are significantly lower than those of DCIS lesions.[1,6,15,16]

[1]Department of Diagnostic Radiology, Tohoku University Graduate School of Medicine, Miyagi, Japan
[2]Department of Surgical Oncology, Tohoku University Graduate School of Medicine, Miyagi, Japan
[3]Department of Orthopaedic Surgery, Tohoku University Graduate School of Medicine, Miyagi, Japan
[4]Department of Radiological Technology, Tohoku University Graduate School of Medicine, Miyagi, Japan

[*]Corresponding author: Department of Diagnostic Radiology, Tohoku University Graduate School of Medicine, 1-1 Seiryo, Sendai, Miyagi 980-8574, Japan. Phone: +81-22-717-7312, Fax: +81-22-717-7316, E-mail: naokomori7127@gmail.com

Received: December 20, 2019 | Accepted: February 4, 2020

With respect to the DWI scan protocol, single-shot echo-planar imaging (EPI) is generally used. Although EPI-DWI is a fast scanning technique with high signal-to-noise ratio (SNR), it sometimes encounters difficulty in calculating the ADC in breast lesions.[17] EPI-DWI is prone to susceptibility artifacts due to field inhomogeneities.[18] Fatty components adjoining or within the breast lesions and complex structure with boundary between the air and the surface of the breast can cause susceptibility artifacts and prevent the precise measurement of the ADC values.[6,17]

Diffusion-weighted imaging with the turbo spin-echo (TSE) technique (TSE-DWI) using radio-frequency (RF) refocusing pulses has been proposed as an alternative to the above.[19–21] TSE-DWI is less sensitive to susceptibility artifacts than EPI-DWI, although its SNR is lower and scan time longer than those of EPI-DWI owing to multiple RF refocusing pulses.[22] To detect cholesteatomas in the middle ear, TSE-DWI provides excellent sensitivity and specificity compared with EPI-DWI.[23] The effectiveness of EPI-DWI is limited when applied to the middle ear because of susceptibility artifacts caused by field inhomogeneities at the boundary between air and bone.[24] With respect to breast tumors, Baltzer et al.[21] reported that TSE-DWI could be useful to detect lesions and measure ADC values. Similar to the middle ear, TSE-DWI might also be effective for the evaluation of breast lesions because the breast contains different types of tissues, such as breast parenchyma, fatty components, carcinoma, and the breast surface. To the best of our knowledge, no report has assessed the diagnostic performance of TSE-DWI in terms of differentiating DCIS from IDC lesions. Furthermore, the appropriate ADC parameter of TSE-DWI for differentiation between DCIS and IDC lesions has not been validated by histogram analysis. Previous study showed that mean ADC values of IDC lesions were significantly lower than that of DCIS lesions.[16] While, Kim et al.[25] used histogram analysis and showed that 5th percentile ADC value could be helpful for differentiating low-risk from non-low-risk DCIS lesions. Histogram analysis might be effective to validate the appropriate ADC parameter in differentiating DCIS from IDC lesions.

The purpose of this study was to compare the image quality between TSE-DWI and EPI-DWI, and to validate the diagnostic performance of the ADC parameters of the two techniques by using histogram analysis in terms of differentiation between DCIS and IDC lesions.

Materials and Methods

Patients

Our Institutional Review Board approved this retrospective study and waived the informed consent requirement. We retrospectively reviewed breast magnetic resonance imaging (MRI) studies performed at our institution between November 2014 and July 2016. A total of 119 consecutive patients with lesions diagnosed as invasive carcinoma of no-special type by mastectomy or lumpectomy, underwent preoperative breast MRI. Special histological types were excluded because their management was determined according to their individual biological features rather than whether the relevant lesion was DCIS or IDC. We also excluded the following patients (Fig. 1): (a) patients who had undergone neoadjuvant chemotherapy ($n = 19$) and whose purpose of MRI examination was the evaluation of recurrence after surgery ($n = 2$), because the image quality and diagnostic performance of TSE-DWI and EPI-DWI should be compared in an untreated setting; (b) patients with a too small or thin lesion to perform segmentation, thus precluding the measurement of ADC values ($n = 2$); (c) patients with suboptimal DWI owing to susceptibility artifact because of placement of a metallic clip ($n = 1$); and (d) patients with neither enhancement on dynamic contrast-enhanced (DCE)-MRI nor high signal intensity on DWI ($n = 1$), because it was impossible to calculate the ADC for such cases. Thus, 94 lesions from 94 patients were included in this study. All patients had undergone mastectomies or lumpectomies, and the surgical specimens were prepared for histological evaluation. The specimens were fixed in a 10% formaldehyde solution, and 2-μm-thick sections were taken every 5 mm. An experienced pathologist evaluated the specimens based on the World Health Organization's histological classification of breast tumors. Of the 94 lesions, 20 were diagnosed as DCIS (lumpectomy: $n = 16$, mastectomy: $n = 4$), and 74 were diagnosed as IDC (lumpectomy: $n = 58$, mastectomy: $n = 16$).

MR image acquisition

A 3T system (Intera Achieva dStream; Philips Healthcare, Best, the Netherlands) with multiple-source radio-frequency transmission was used for MRI. All patients were imaged in the prone position, with both breasts placed into a 16-channel phased array breast coil. The sensitivity encoding (SENSE) technique was used for both TSE-DWI and EPI-DWI as a

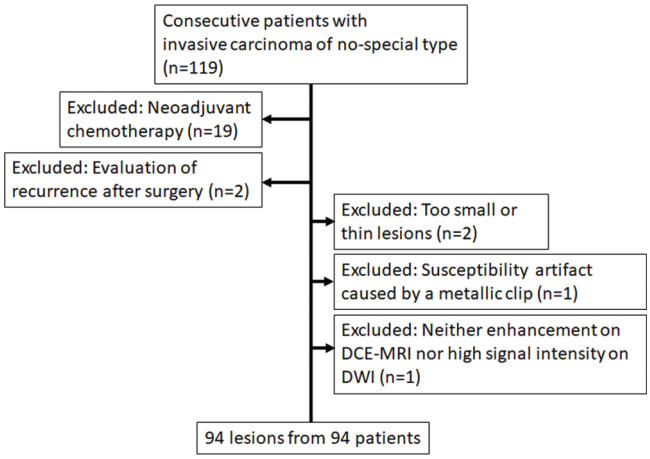

Fig. 1 The flow diagram of patient selection. Twenty-five patients were excluded from a total of 119 consecutive patients, and 94 lesions from 94 patients were included in this study.

parallel imaging method. The MRI protocols consisted of the following sequences: fat-suppressed TSE-DWI with parallel imaging technique [10750/43 (repetition time (ms)/echo time (ms)), field of view 180 × 180 mm, matrix 112 × 88, SENSE factor 2.0, section thickness 5 mm, acquisition time 215 s, fat-suppression spectral attenuated inversion recovery (SPAIR), number of acquisitions (NEX) 4, the application of motion-probing gradient pulse along the *x*, *y*, and *z* directions with *b*-values of 0, 50, and 850 s/mm^2), fat-suppressed EPI-DWI with parallel imaging technique [4987/74 (repetition time (ms)/echo time (ms)), field of view 180 × 180 mm, matrix 112 × 88, SENSE factor 2.0, section thickness 5 mm, acquisition time 324 s, fat suppression SPAIR, NEX 4, and application of motion probing gradient pulse along the *x*, *y*, and *z* directions with *b*-values of 0, 50, 100, 300, 850, and 1000 s/mm^2], DCE-MR images using a three-dimensional (3D) fat-suppressed T_1-weighted gradient-echo sequence [5.3/2.6 (repetition time (ms)/echo time (ms)), field of view 350 × 350 mm, matrix 480 × 277, section thickness 0.9 mm, acquisition time 68 s] with intravenous infusion of 0.1 mmol/kg gadopentetic acid. The scanning of EPI-DWI with *b*-values of 100, 300, and 1000 s/mm^2 was performed for other research purposes. The ADC maps of TSE-DWI and EPI-DWI were formed using the linear regression of logarithmic intensities with *b*-values of 50 and 850 s/mm^2 as follows: ADC = In (*S*1/*S*2)/(*b*2 − *b*1), where *S*1 and *S*2 are the signal intensities in the voxel obtained using different gradient factors (*b*1 = 50 s/mm^2 and *b*2 = 850 s/mm^2).

Image interpretation

The extensions of the lesions, and their diameters and appearance (mass or non-mass) were initially determined according to the American College of Radiology's Breast Imaging Reporting and Data System's MRI criteria,[26] using DCE-MRI by two observers [radiologists (* and **), with *** and **** years of experience in breast MRI, respectively] by consensus. They were blinded to the clinical and pathological information. MRI data for the ADC maps were transferred to a personal computer and processed using Image J software 1.8.0 (https://imagej.nih.gov/ij/).

Image quality of DWI

The overall image quality of TSE-DWI and EPI-DWI was evaluated by one observer (*) in terms of the SNR, contrast-to-noise ratio (CNR), and geometric distortion. To calculate the SNR, regions of interest (ROIs) were placed in areas with homogeneous subcutaneous fat on both TSE-DWI and EPI-DWI (*b* = 850 s/mm^2) so as to be close to the breast cancer lesion as possible because the signal and the noise vary spatially throughout the images in the parallel imaging technique.[27] The number of voxels within the ROI was set to be no smaller than 50 voxels (150 mm^2).[28] The SNR was calculated as follows:[29]

$$\mathrm{SNR} = \frac{S_{fat}}{\rho_{fat}} \quad (1)$$

where S_{fat} indicates the mean signal intensity of the ROI in the area with subcutaneous fat, and ρ_{fat} is the standard deviation of the signal intensity of the ROI.[17]

To calculate the CNR, ROIs of the same size were carefully placed within the breast lesion and normal breast tissue in both TSE-DWI and EPI-DWI (*b* = 850 s/mm^2) so as not to include artifacts. The minimum size of the ROI was 20 mm^2 (six voxels) because the breast lesions and normal breast tissues were often thin or small. The ROIs were placed in the same areas of the TSE-DWI and EPI-DWI as much as was possible, and the CNR was calculated as follows:[30]

$$\mathrm{CNR} = \frac{S_{lesion} - S_t}{\sqrt{(\rho_{lesion})^2 + (\rho_t)^2}} \quad (2)$$

where S_{lesion} indicates the mean signal intensity of the ROI placed in the lesion, S_t indicates the mean signal intensity of the ROI placed in the normal breast tissue, ρ_{lesion} indicates the standard deviation of the ROI placed in the lesion, and ρ_t indicates the standard deviation of the ROI placed in the normal breast tissue. The solid area of normal breast tissues were carefully selected to place ROIs.

Geometric distortion was measured in TSE-DWI and EPI-DWI (*b* = 850 s/mm^2) with reference to undistorted DCE-MR images. Two matching anatomic sites were used: one was the site of the lesion closest to the skin, and the other was the site of the skin closest to the lesion. These two sites were identified in images of the TSE-DWI (*b* = 850 s/mm^2), EPI-DWI (*b* = 850 s/mm^2) and DCE-MR images, respectively (Figs. 2a–2c). The distance between the sites was calculated in images of the TSE-DWI, EPI-DWI, and DCE-MR images for each patient as $\mathrm{Distance}_{\mathrm{TSE}}$, $\mathrm{Distance}_{\mathrm{EPI}}$, and $\mathrm{Distance}_{\mathrm{DCE\text{-}MRI}}$, respectively. Then, the geometric distortions of TSE-DWI and EPI-DWI were calculated using the absolute values of the difference between $\mathrm{Distance}_{\mathrm{DCE\text{-}MRI}}$ and $\mathrm{Distance}_{\mathrm{TSE}}$ or $\mathrm{Distance}_{\mathrm{EPI}}$ as follows:

$$\text{Geometric distortion of TSE-DWI} = \frac{|\mathrm{Distance}_{\mathrm{TSE}} - \mathrm{Distance}_{\mathrm{DCE\text{-}MRI}}|}{\mathrm{Distance}_{\mathrm{DCE\text{-}MRI}}} \quad (3)$$

$$\text{Geometric distortion of EPI-DWI} = \frac{|\mathrm{Distance}_{\mathrm{EPI}} - \mathrm{Distance}_{\mathrm{DCE\text{-}MRI}}|}{\mathrm{Distance}_{\mathrm{DCE\text{-}MRI}}} \quad (4)$$

These image quality metrics were compared between TSE-DWI and EPI-DWI on each lesion.

Histogram analysis of whole tumor volume

A histogram analysis of the voxel-based data of whole tumor volume was performed. Segmentation covering as much as possible of the tumor was performed manually on each slice of the ADC maps of TSE-DWI and EPI-DWI (Figs. 3a and 3c) with reference to TSE-DWI (*b* = 850 s/mm^2; Fig. 3b), EPI-DWI (*b* = 850 s/mm^2; Fig. 3d), and DCE-MRI (Fig. 3e). The voxel-based ADC data of each slice were summed to obtain the voxel-based ADC data of

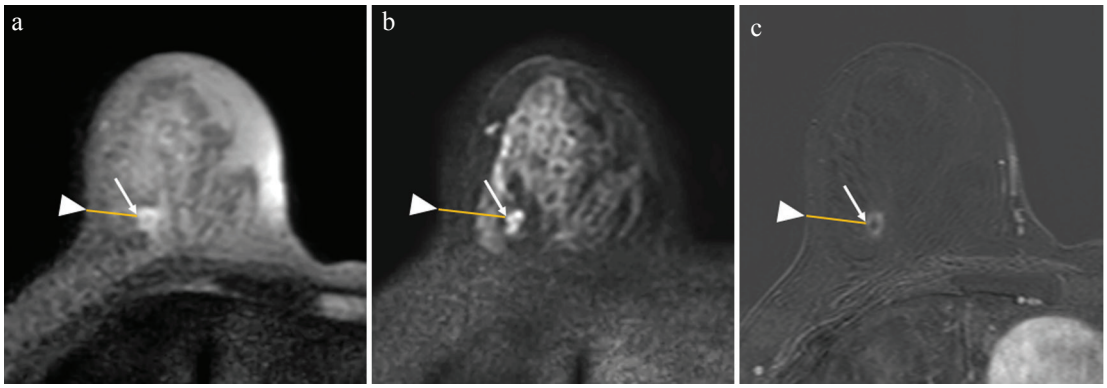

Fig. 2 A 60-year-old woman diagnosed with right-invasive ductal carcinoma by lumpectomy. The methods used to evaluate geometric distortion in TSE-DWI and EPI-DWI. Two matching anatomic sites were used: the site of the lesion closest to the skin (arrows), and the site of the skin closest to the lesion (arrowheads). The distance between the sites was calculated as $Distance_{TSE}$ in images of TSE-DWI (b = 850 s/mm^2) (**a**), $Distance_{EPI}$ in those of EPI-DWI (b = 850 s/mm^2) (**b**), and $Distance_{DCE\text{-}MRI}$ in those of DCE-MR (**c**). In this case, $Distance_{TSE}$, $Distance_{EPI}$, and $Distance_{DCE\text{-}MRI}$ were 19.1, 25.3, and 19.5 mm, respectively. The geometric distortions of TSE-DWI and EPI-DWI were 0.021 and 0.29, respectively. TSE, turbo spin-echo; DWI, diffusion-weighted imaging; EPI, echo-planar imaging.

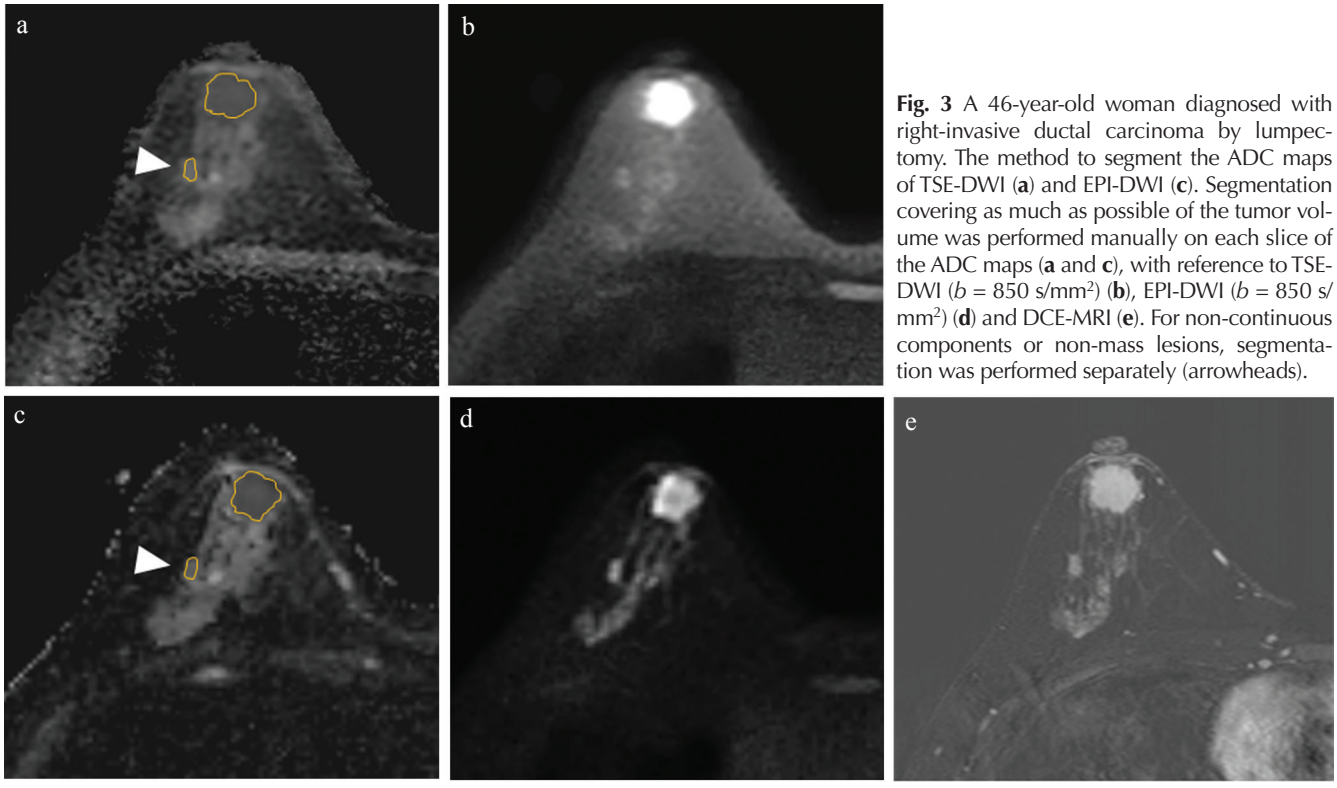

Fig. 3 A 46-year-old woman diagnosed with right-invasive ductal carcinoma by lumpectomy. The method to segment the ADC maps of TSE-DWI (**a**) and EPI-DWI (**c**). Segmentation covering as much as possible of the tumor volume was performed manually on each slice of the ADC maps (**a** and **c**), with reference to TSE-DWI (b = 850 s/mm^2) (**b**), EPI-DWI (b = 850 s/mm^2) (**d**) and DCE-MRI (**e**). For non-continuous components or non-mass lesions, segmentation was performed separately (arrowheads).

whole tumor volume. For non-continuous components or non-mass lesions, segmentation was performed separately for individual components within the contour and summed (Figs. 3a and 3c). The voxel-based ADC data of whole tumor volume was obtained for TSE-DWI and EPI-DWI separately. The histograms were obtained from the voxel-based ADC data of whole tumor volume (Fig. 4a), and the cumulative frequency distributions were plotted with the ADC values on the x-axis and the percentage of cumulative frequency on the y-axis (Fig. 4b). The 10th, 25th, 50th, 75th, and 90th percentiles were derived from the cumulative frequency distributions of the voxel-based ADC data of whole tumor volume in TSE-DWI and EPI-DWI, respectively. All segmentation was performed by the two observers independently, and the interobserver reliability of the percentiles of TSE-DWI and EPI-DWI between the observers was analyzed using the interclass correlation coefficient (ICC). Each percentile value of the voxel-based ADC data of whole tumor volume of TSE-DWI and EPI-DWI was compared between DCIS and IDC lesions.

Statistical analysis

The Mann–Whitney *U*-test was used to compare the age, lesion diameter, and the percentile values of the voxel-based ADC data of whole tumor volume in TSE-DWI and EPI-DWI between DCIS and IDC lesions. Fisher's exact test was used for comparing lesion appearance and the immunohistochemical findings for the tumor between DCIS and IDC lesions. The Wilcoxon signed-rank test was used to compare TSE-DWI and EPI-DWI in terms of the SNR, CNR, and geometric distortion for each patient. The interobserver reliability of the ADC measurements was assessed using ICCs. A value of *r* of one was deemed to indicate perfect agreement, 0.81–0.99 to represent almost perfect agreement, 0.61–0.80 to represent substantial agreement, 0.41–0.60 to represent moderate agreement, 0.21–0.40 to represent fair agreement, and 0.20 or less to represent slight agreement.[31] The effectiveness of each percentile of the voxel-based ADC data of whole tumor volume in TSE-DWI and EPI-DWI in terms of differentiating between DCIS and IDC lesions was evaluated using the receiver-operating-characteristic (ROC) analysis and area under the ROC curve (AUC). The AUCs were compared among the percentile values of the voxel-based ADC data of whole tumor volume in TSE-DWI and EPI-DWI. Statistical analyses were performed using JMP Pro 14 (SAS Institute, Cary, NC, USA). The *P*-values <0.05 were deemed to indicate statistical significance. We mainly compared five percentile ADC values (10th, 25th, 50th, 75th, and 90th percentiles) from TSE-DWI and EPI-DWI, respectively. Therefore, we performed Bonferroni correction of 10 multiple comparisons, and after the Bonferroni correction of 10 multiple comparisons, the critical value was <0.005 (0.05/10).

Results

There was no significant difference between DCIS and IDC lesions in terms of age and diameter (Table 1). The IDC lesions were evaluated as mass appearance in significantly higher prevalence than DCIS lesions ($P < 0.0001$;

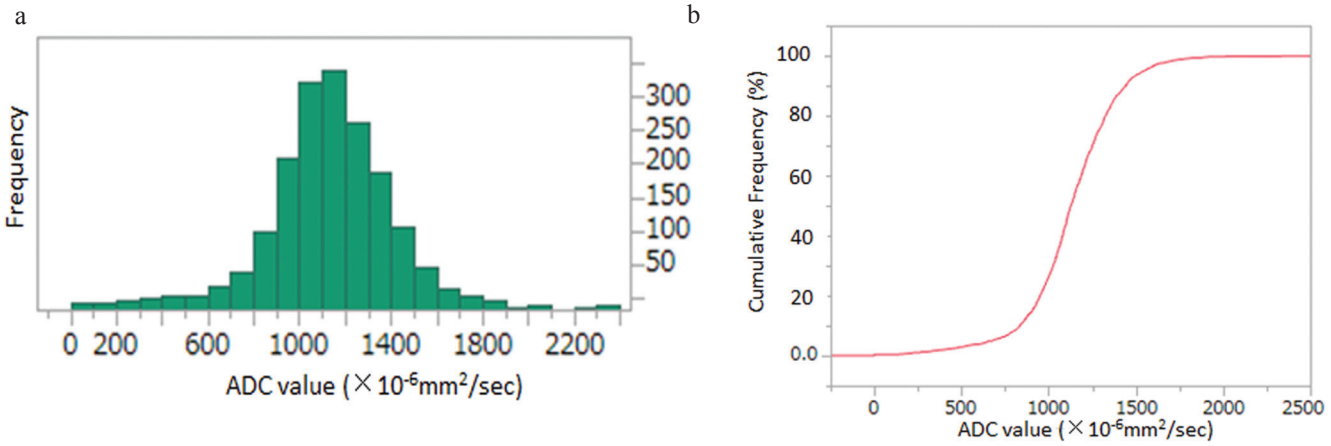

Fig. 4 The method used to obtain percentile ADC values from histogram analysis. The ADC histogram is plotted with ADC values on the *x*-axis and the number of voxels on the *y*-axis (**a**). The curved line in red represents the relative cumulative frequency of voxels (i.e., the percentage of the number of cumulative voxels at each ADC value of the total number of voxels analyzed). The ADC values of the 10th, 25th, 50th, 75th, and 90th percentiles were obtained from the curve.

Table 1 Characteristics of the background of patients and lesions

Variables	DCIS (*n* = 20)	IDC (*n* = 74)	*P*-value
Age (years): Median (range)	56 (44–78)	61 (32–87)	0.16
Lesion diameter (mm): Median (range)	29 (6–54)	19.5 (7–100)	0.13
Lesion appearance [*n* (%)]			
Mass	7 (35)	63 (85)	<0.0001
Non-mass	13 (65)	11 (15)	
Immunohistochemical findings of tumor [*n* (%)]			
Estrogen receptor (positive/negative)	19 (95)/1 (5)	69 (93)/5 (7)	0.77
Progesteron receptor (positive/negative)	16 (80)/4 (20)	64 (86)/10 (14)	0.46
HER2 (positive/negative)	N/A	7 (9)/67 (91)	N/A
Van Nuys grades of DCIS/Nottingham histologic grades (%) of IDC	Grade 1: 7 (35) Grade 2: 10 (50) Grade 3: 3 (15)	Grade 1: 33 (45) Grade 2: 32 (43) Grade 3: 9 (12)	N/A

Table 1). There was no significant difference between the DCIS and IDC lesions in terms of the status of estrogen or the progesterone receptor (Table 1). HER2 positivity was not evaluated in the DCIS lesions. The Van Nuys grades of DCIS and Nottingham histologic grades of IDC are shown in Table 1. For the evaluation of the image quality, the SNR and CNR of TSE-DWI were significantly higher than those of EPI-DWI ($P < 0.0001$ and < 0.0001, respectively) (Table 2). The geometric distortion in TSE-DWI was significantly lower than that in EPI-DWI ($P < 0.0001$; Table 2). In TSE-DWI, ICC of 10th, 25th, 50th, 75th and 90th percentile values were 0.64, 0.71, 0.71, 0.69, and 0.65, respectively, indicating substantial agreement. The 10th, 25th, 50th and 75th percentile values of ADC data of TSE-DWI were significantly different between the DCIS and IDC lesions ($P = 0.0010$, 0.0004, 0.0008, and 0.0044, respectively) (Table 3). The AUCs of the ROC curve analysis were 0.74, 0.75, 0.74, and 0.70 for the 10th, 25th, 50th, and 75th percentile values, respectively. In EPI-DWI, ICC of 10th, 25th, 50th, 75th and 90th percentile values were 0.70, 0.67, 0.75, 0.75, and 0.75, respectively, indicating substantial agreement. The 50th and 75th percentile values of ADC data of EPI-DWI were significantly different between the DCIS and IDC lesions ($P = 0.0009$ and 0.0093, respectively) (Table 4). The AUCs of the ROC curve analysis were 0.74 and 0.69 for the 50th and 75th percentile values, respectively. There was no significant difference among the AUCs in the ROC curve analysis for 10th, 25th, 50th and 75th percentile values of TSE-DWI, and the 50th and 75th percentile values of EPI-DWI ($P = 0.29$).

Table 2 Comparison of image quality between TSE-DWI and EPI-DWI

	TSE-DWI	EPI-DWI	*P*-value
Signal-to-noise ratio (SNR)	14.8 ± 5.3	6.9 ± 1.9	<0.0001
Contrast-to-noise ratio (CNR)	5.4 ± 4.7	3.5 ± 3.0	<0.0001
Geometric distortion	0.07 ± 0.07	0.23 ± 0.34	<0.0001

Data was expressed as means ± standard deviation.

Discussion

Our study showed that the image quality of TSE-DWI was significantly better than that of EPI-DWI. Previous study reported that the SNR of TSE-DWI was lower than that of EPI-DWI owing to multiple RF refocusing pulses;[21] however, the image quality of TSE-DWI has been recently improved by using the modulus averaging method, short RF pulses, and SENSE.[22,32] Our results are attributable to the high SNR achieved by these factors. To calculate the SNR, ROIs were placed in the areas with homogeneous subcutaneous fat in both TSE-DWI and EPI-DWI ($b = 850$ s/mm^2). Although the method of fat suppression might have affected the measurement of SNR in areas with fat, the same fat suppression method (SPAIR) was used on both TSE-DWI and EPI-DWI images. Regarding the CNR, which is a quantitative parameter representing the visibility of lesions, previous studies have reported that the visibility of lesions was better in EPI-DWI than in TSE-DWI using the 1.5T MR system.[21] Using our 3T MR system, the CNR was significantly higher

Table 3 Diagnostic performance to differentiate between ductal carcinoma *in situ* (DCIS) and invasive ductal carcinoma (IDC) using percentile ADC values of TSE-DWI

(× 10^6 mm^2/s)	DCIS ($n = 20$)	IDC ($n = 74$)	ICC	*P*-value	AUC
10th percentile	1034 ± 171	859 ± 223	0.64 (0.40, 0.78)	0.0010*	0.74
25th percentile	1143 ± 186	962 ± 204	0.71 (0.52, 0.82)	0.0004*	0.75
50th percentile	1252 ± 199	1076 ± 210	0.71 (0.52, 0.83)	0.0008*	0.74
75th percentile	1356 ± 210	1196 ± 231	0.69 (0.49, 0.81)	0.0044*	0.70
90th percentile	1463 ± 238	1329 ± 280	0.65 (0.41, 0.78)	0.031	N/A

Data was expressed as means ± standard deviation.

Table 4 Diagnostic performance to differentiate between ductal carcinoma *in situ* (DCIS) and invasive ductal carcinoma (IDC) using percentile ADC values of EPI-DWI

(× 10^6 mm^2/s)	DCIS ($n = 20$)	IDC ($n = 74$)	ICC	*P*-value	AUC
10th percentile	786 ± 323	723 ± 286	0.70 (0.48, 0.83)	0.43	N/A
25th percentile	1063 ± 234	915 ± 252	0.67 (0.44, 0.81)	0.012	N/A
50th percentile	1322 ± 238	1108 ± 256	0.75 (0.57, 0.86)	0.0009*	0.74
75th percentile	1549 ± 298	1344 ± 281	0.75 (0.58, 0.86)	0.0093*	0.69
90th percentile	1761 ± 333	1604 ± 344	0.75 (0.57, 0.86)	0.052	N/A

Data was expressed as means ± standard deviation.

in TSE-DWI than in EPI-DWI, and this result is also attributable to the improved SNR.

Geometric distortion was significantly lower in TSE-DWI than in EPI-DWI in our study. The susceptibility artifacts of EPI-DWI cause geometric distortions and signal loss, leading to low values of the SNR and CNR.[18] The stronger geometric distortion in EPI-DWI might be one reason for why the CNR and SNR of EPI-DWI were significantly lower than those of TSE-DWI. In order to evaluate geometric distortion, we used the DCE-MR images as undistorted reference images in this study. Although the DCE-MR images were scanned using a 3D fat-suppressed T_1-weighted gradient-echo sequence, the slice thickness and sequence of which were different from those of EPI-DWI and TSE-DWI, DCE-MR images are generally used as reference to segment ADC maps to diagnose breast cancer. Therefore, we used DCE-MR images as undistorted references.

In this study, segmentation was performed manually on each slice of the ADC maps of TSE-DWI and EPI-DWI with reference to DCE-MRI separately, and interobserver reliability attained substantial agreement in all percentile values in TSE-DWI and EPI-DWI. In EPI-DWI, the manual correction of the segmentation was needed to cover the lesion precisely because of geometric distortion. Thus, the segmentation in each case was different between TSE-DWI and EPI-DWI, and such a difference might have affected the results of the two methods. In the future, automatic segmentation will be needed to compare the diagnostic performance of the two methods.

For diagnostic performance in differentiating between DCIS and IDC lesions, four percentile values (10th, 25th, 50th, and 75th) of TSE-DWI were significantly different between the two groups, while only the 50th and 75th percentile values of EPI-DWI were significantly different between the groups. The presence of geometric distortion leading to more noise with low SNR and CNR in EPI-DWI might prevent the accurate calculation of the ADC values. This is why only the 50th and 75th percentile values of EPI-DWI were significantly different between the DCIS and IDC lesions. TSE-DWI with a smaller geometric distortion achieved a high SNR and CNR, on the contrary. We speculated that the wider diagnostic window of TSE-DWI with the 10th, 25th, 50th, and 75th percentile values might have been obtained owing to the high SNR and CNR.

We used the histogram analysis to compare the range of percentile values with diagnostic performance between TSE-DWI and EPI-DWI. Therefore, we did not use kurtosis or skewness of histogram analysis as well as mean ADC value. Furthermore, manual ROI placement to obtain mean ADC value was not performed because it is currently out of the scope of our study to compare the percentile ADC values with the mean ADC value obtained from manual ROI placement. In this study, 50th and 75th percentile ADC values of IDC lesions were significantly lower than those of DCIS lesions in EPI-DWI. We suppose that our study might support the results of previous study reporting that mean ADC values of IDC lesions were significantly lower than that of DCIS lesions in EPI-DWI.[16]

In this study, the diagnostic performance of TSE-DWI in terms of percentile ADC values was not significantly different from that of EPI-DWI: The AUC of the ROC curve analysis was not significantly different between the percentile values of TSE-DWI and EPI-DWI. The severe geometric distortion of EPI-DWI was often observed in lesions close to the skin or the nipple (Fig. 5). For such lesions, TSE-DWI might be more effective, and further research involving a subgroup analysis with different orientations of the lesion is needed in the future.

One of the disadvantages of TSE-DWI is the longer scan time than EPI-DWI even though the diagnostic performance in differentiating DCIS form IDC was not significantly different between the two methods. However, we suppose that TSE-DWI could be added to the breast MRI protocol depending on cases; if there is a severe distortion within or around the lesion in EPI-DWI, additional TSE-DWI scanning could be performed.

This study had several limitations. First, the sample size was small. Second, this study was retrospective for patients with lesions diagnosed as breast carcinoma, not otherwise

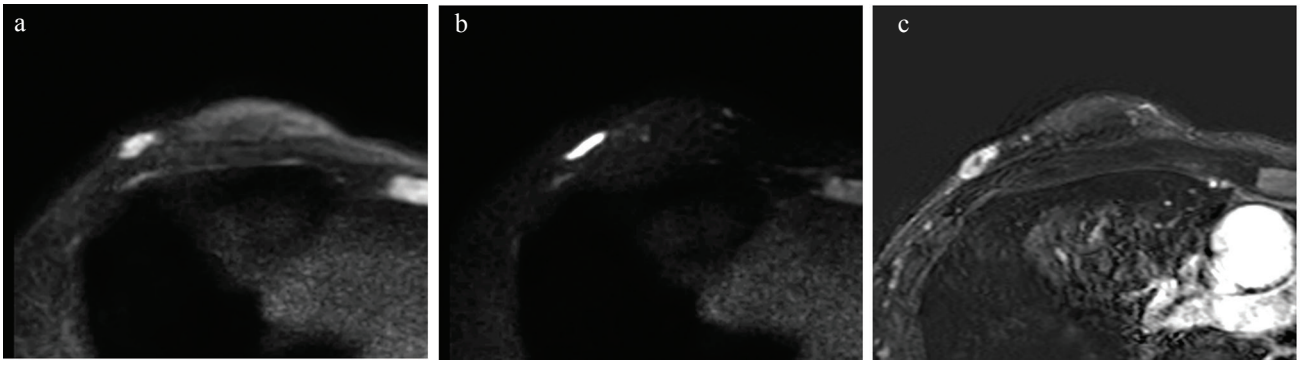

Fig. 5 A 37-year-old woman diagnosed with right-invasive ductal carcinoma by lumpectomy. The mass is close to the skin and with reference to DCE-MRI (**c**), it is severely distorted in EPI-DWI (b = 850 s/mm^2) (**b**) compared to TSE-DWI (b = 850 s/mm^2) (**a**). The geometric distortion of TSE-DWI (0.139) is lower than that of EPI-DWI (0.479).

specified (NOS) by mastectomy or lumpectomy. To verify the effectiveness of TSE-DWI in comparison with EPI-DWI in terms of differentiation between DCIS and IDC lesions, a prospective study might be needed in the future. Third, the spatial resolution of both TSE-DWI and EPI-DWI was inadequate. For non-mass lesions, segmentation was performed separately for small individual components, and two patients were excluded because of lesions that were too small or thin to perform segmentation. The development of imaging techniques with higher spatial resolution of DWI is needed in the future to solve this problem. Fourth, the imaging technique of TSE-DWI has not yet been standardized. Bogner et al.[33] showed that appropriate *b*-values for the 3T system to evaluate the ADC in EPI-DWI to distinguish between benign and malignant tumors are 50 and 850 s/mm^2. To the best of our knowledge, appropriate *b*-values to calculate ADC for TSE-DWI have not yet been determined. Ei Khouli et al.[34] reported that grandular tissue-normalized ADC improves the characterization of breast lesions. The normalization of the ADC in TSE-DWI as well as EPI-DWI should be studied in future work. Fifth, there were cases with incomplete fat suppression in TSE-DWI (n = 22): signal intensity of fat area was higher than that of breast tissue in such cases (Fig. 2a). The inversion time (TI) delay of SPAIR pulse may not have been appropriate in TSE-DWI, and a further study will be needed to improve the quality of fat suppression in TSE-DWI. Sixth, we could not compare the scan time between TSE-DWI (215 s) and EPI-DWI (324 s), because the numbers of *b*-values were different (TSE-DWI with *b*-values of 0, 50, and 850 s/mm^2 and EPI-DWI with *b*-values of 0, 50, 100, 300, 850, and 1000 s/mm^2). However, the scan time of EPI-DWI with *b*-values of 0, 50, and 850 s/mm^2 was estimated as 114 s, which was shorter than TSE-DWI with the same *b*-values (215 s). Further technical development to resolve the longer scan time of TSE-DWI will be needed.

In conclusion, the image quality of TSE-DWI was significantly better than that of EPI-DWI. The diagnostic performance to differentiate DCIS from IDC lesions was observed with a wider range of percentile values in TSE-DWI than EPI-DWI, although the diagnostic performance as assessed using the AUCs of ROC curve analysis was not significantly different between TSE-DWI and EPI-DWI.

Funding

This research was supported by JSPS KAKENHI (Grant numbers 15K09913, 19K17159 and 18K07742).

Acknowledgments

The authors thank Mari Yamaoka, Hiroki Ichida, Takuro Kuwano, Kenta Kubota, Tomohiro Yamada, Mayu Sawaguchi, Naoko Hirose, Kanako Shibui, Yo Oguma and Kyuhei Takahashi in Tohoku University for their kind support.

Conflicts of Interest

The authors declare that they have no conflicts of interest.

References

1. Iima M, Le Bihan D, Okumura R, et al. Apparent diffusion coefficient as an MR imaging biomarker of low-risk ductal carcinoma in situ: a pilot study. Radiology 2011; 260: 364–372.
2. Sugahara T, Korogi Y, Kochi M, et al. Usefulness of diffusion-weighted MRI with echo-planar technique in the evaluation of cellularity in gliomas. J Magn Reson Imaging 1999; 9:53–60.
3. Pinker K, Bickel H, Helbich TH, et al. Combined contrast-enhanced magnetic resonance and diffusion-weighted imaging reading adapted to the "Breast Imaging Reporting and Data System" for multiparametric 3-T imaging of breast lesions. Eur Radiol 2013; 23:1791–1802.
4. Kuroki Y, Nasu K, Kuroki S, et al. Diffusion-weighted imaging of breast cancer with the sensitivity encoding technique: analysis of the apparent diffusion coefficient value. Magn Reson Med Sci 2004;3:79–85.
5. Mori N, Mugikura S, Takasawa C, et al. Peritumoral apparent diffusion coefficients for prediction of lymphovascular invasion in clinically node-negative invasive breast cancer. Eur Radiol 2016; 26:331–339.
6. Mori N, Ota H, Mugikura S, et al. Detection of invasive components in cases of breast ductal carcinoma in situ on biopsy by using apparent diffusion coefficient MR parameters. Eur Radiol 2013; 23:2705–2712.
7. Woodhams R, Kakita S, Hata H, et al. Diffusion-weighted imaging of mucinous carcinoma of the breast: evaluation of apparent diffusion coefficient and signal intensity in correlation with histologic findings. AJR Am J Roentgenol 2009; 193:260–266.
8. Onishi N, Kanao S, Kataoka M, et al. Apparent diffusion coefficient as a potential surrogate marker for Ki-67 index in mucinous breast carcinoma. J Magn Reson Imaging 2015;41:610–615.
9. Park SH, Moon WK, Cho N, et al. Diffusion-weighted MR imaging: pretreatment prediction of response to neoadjuvant chemotherapy in patients with breast cancer. Radiology 2010; 257:56–63.
10. Jensen LR, Garzon B, Heldahl MG, Bathen TF, Lundgren S, Gribbestad IS. Diffusion-weighted and dynamic contrast-enhanced MRI in evaluation of early treatment effects during neoadjuvant chemotherapy in breast cancer patients. J Magn Reson Imaging 2011;34:1099–1109.
11. Richard R, Thomassin I, Chapellier M, et al. Diffusion-weighted MRI in pretreatment prediction of response to neoadjuvant chemotherapy in patients with breast cancer. Eur Radiol 2013; 23:2420–2431.
12. Goyal A, Douglas-Jones A, Monypenny I, Sweetland H, Stevens G, Mansel RE. Is there a role of sentinel lymph node biopsy in ductal carcinoma in situ?: analysis of 587 cases. Breast Cancer Res Treat 2006; 98:311–314.
13. Huo L, Sneige N, Hunt KK, Albarracin CT, Lopez A, Resetkova E. Predictors of invasion in patients with core-needle biopsy-diagnosed ductal carcinoma in situ and recommendations

for a selective approach to sentinel lymph node biopsy in ductal carcinoma in situ. Cancer 2006; 107:1760–1768.
14. Hung WK, Ying M, Chan M, Mak KL, Chan LK. The impact of sentinel lymph node biopsy in patients with a core biopsy diagnosis of ductal carcinoma in situ. Breast Cancer 2010; 17:276–280.
15. Choi SY, Chang YW, Park HJ, Kim HJ, Hong SS, Seo DY. Correlation of the apparent diffusion coefficiency values on diffusion-weighted imaging with prognostic factors for breast cancer. Br J Radiol 2012;85:e474–e479.
16. Yoshikawa MI, Ohsumi S, Sugata S, et al. Comparison of breast cancer detection by diffusion-weighted magnetic resonance imaging and mammography. Radiat Med 2007; 25:218–223.
17. Partridge SC, Nissan N, Rahbar H, Kitsch AE, Sigmund EE. Diffusion-weighted breast MRI: Clinical applications and emerging techniques. J Magn Reson Imaging 2017; 45:337–355.
18. Bogner W, Pinker-Domenig K, Bickel H, et al. Readout-segmented echo-planar imaging improves the diagnostic performance of diffusion-weighted MR breast examinations at 3.0 T. Radiology 2012; 263:64–76.
19. Raza S, Vallejo M, Chikarmane SA, Birdwell RL. Pure ductal carcinoma in situ: a range of MRI features. AJR Am J Roentgenol 2008; 191:689–699.
20. Kinoshita T, Yashiro N, Ihara N, Funatu H, Fukuma E, Narita M. Diffusion-weighted half-Fourier single-shot turbo spin echo imaging in breast tumors: differentiation of invasive ductal carcinoma from fibroadenoma. J Comput Assist Tomogr 2002; 26:1042–1046.
21. Baltzer PA, Renz DM, Herrmann KH, et al. Diffusion-weighted imaging (DWI) in MR mammography (MRM): clinical comparison of echo planar imaging (EPI) and half-Fourier single-shot turbo spin echo (HASTE) diffusion techniques. Eur Radiol 2009; 19:1612–1620.
22. Mikayama R, Yabuuchi H, Sonoda S, et al. Comparison of intravoxel incoherent motion diffusion-weighted imaging between turbo spin-echo and echo-planar imaging of the head and neck. Eur Radiol 2018; 28:316–324.
23. Verhappen MH, Pouwels PJ, Ljumanovic R, et al. Diffusion-weighted MR imaging in head and neck cancer: comparison between half-fourier acquired single-shot turbo spin-echo and EPI techniques. AJNR Am J Neuroradiol 2012; 33: 1239–1246.
24. De Foer B, Vercruysse JP, Pilet B. Single-shot, turbo spin-echo, diffusion-weighted imaging versus spin-echo-planar, diffusion-weighted imaging in the detection of acquired middle ear cholesteatoma. AJNR Am J Neuroradiol 2006; 27:1480–1482.
25. Kim JY, Kim JJ, Lee JW, et al. Risk stratification of ductal carcinoma in situ using whole-lesion histogram analysis of the apparent diffusion coefficient. Eur Radiol 2019; 29:485–493.
26. American College of Radiology. Breast imaging reporting and data system (BI-RADS), 5th ed. Reston. American College of Radiology, 2013.
27. Heverhagen JT. Noise measurement and estimation in MR imaging experiments. Radiology 2007; 245:638–639.
28. Ogura A, Miyati T, Kobayashi M, et al. [Method of SNR determination using clinical images]. Jpn J Radiol Technol 2007; 63:1099–1104 (in Japanese).
29. Kaufman L, Kramer DM, Crooks LE, Ortendahl DA. Measuring signal-to-noise ratios in MR imaging. Radiology 1989; 173:265–267.
30. Song X, Pogue BW, Tosteson TD. Automated region detection based on the contrast-to-noise ratio in near-infrared tomography. Appl Opt 2004; 43:1053–1062.
31. Landis JR, Koch GG. The measurement of observer agreement for categorical data. Biometrics 1977; 33: 159–174.
32. Yoshida T, Urikura A, Shirata K, Nakaya Y, Terashima S, Hosokawa Y. Image quality assessment of single-shot turbo spin echo diffusion-weighted imaging with parallel imaging technique: a phantom study. Br J Radiol 2016; 89:20160512.
33. Bogner W, Gruber S, Pinker K, et al. Diffusion-weighted MR for differentiation of breast lesions at 3.0 T: how does selection of diffusion protocols affect diagnosis? Radiology 2009; 253:341–351.
34. Ei Khouli RH, Jacobs MA, Mezban SD, et al. Diffusion-weighted imaging improves the diagnostic accuracy of conventional 3.0-T breast MR imaging. Radiology 2010; 256:64–73.